

COMPUTATIONAL INVESTIGATION OF AN OSCILLATING COMPRESSOR CASCADE EXPERIMENT

9TH SYMPOSIUM ON UNSTEADY AERODYNAMICS, AEROACOUSTICS AND AEROELASTICITY OF TURBOMACHINES (ISUAAT)

Gerhard Kahl
MTU Aero Engines
P.O. Box 50 06 40
D-80976 Munich, Germany

Holger Hennings
DLR Institute of Aeroelasticity
Bunsenstr. 10
D-37073 Göttingen, Germany

1 Abstract

Computational fluid dynamics are applied to an oscillating compressor cascade experiment to gain further understanding of the flow field details and to assess the capability of the methods employed to model the relevant physics of the experiment.

Previous unsteady two-dimensional Navier-Stokes calculations for this experiment have captured the global trends of the aeroelastic stability of the cascade, but have also highlighted severe problems in modelling the steady flow fields, resulting in considerable deviations of the calculated unsteady pressure magnitudes from the measured ones. In the present paper, the effects of three-dimensionality, viscosity, tip leakage, boundary conditions and leakage flows are studied. It is found that a small secondary inflow (approx. 1.5% of the total massflow) has an overwhelming influence on the overall flowfield. Unsteady computations with and without this secondary inflow highlight the importance of using the correct steady base flow to achieve good unsteady results.

2 Introduction

Over the last decades, much work has been done on the development of sophisticated calculation methods for unsteady flows in turbomachinery. Meanwhile, 3D unsteady calculations are routinely used by almost all major engine manufacturers. At the same time, the open sources of good, well documented experimental data to calibrate these methods have

remained fairly limited, for example to the well-known “Lausanne Standard Configurations” [3]. DLR and MTU have set up a joint effort to generate high-quality experimental data for compressor cascade undergoing torsional oscillations [1,7]. While generating calibration data for the computational methods is a major goal of this project, it further aims to improve the understanding of compressor torsional flutter at sub- and transonic Mach numbers, high incidence and fairly high oscillation amplitudes. By means of teaming of the resources at DLR and MTU, the transfer of research know-how from academia to industry was significantly improved, while at the same time the detailed feed-back on the current industrial design requirements and problem areas gives the research establishments the possibility to focus their work on these tasks and consequently improve the productivity of their work.

3 Experimental Set-up

The experimental investigations have been performed in the annular cascade tunnel at the École Polytechnique Federale de Lausanne (EPFL). In the past 15 years, much experimental work has been done there measuring unsteady pressure distributions in compressor and in turbine cascades, e.g. [10,11].

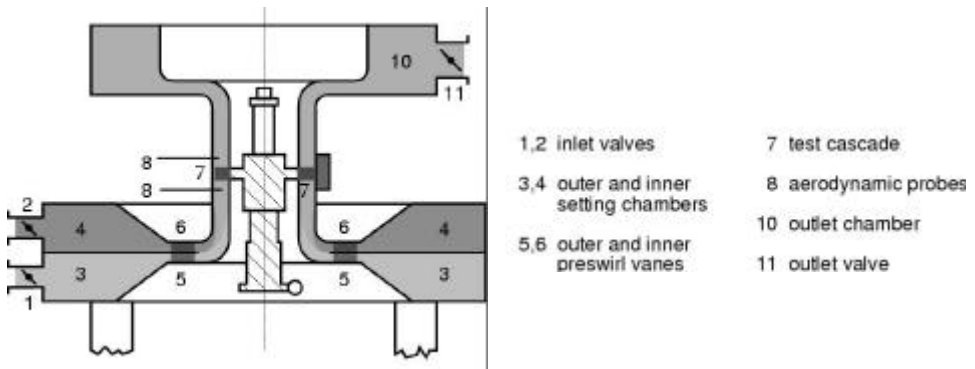
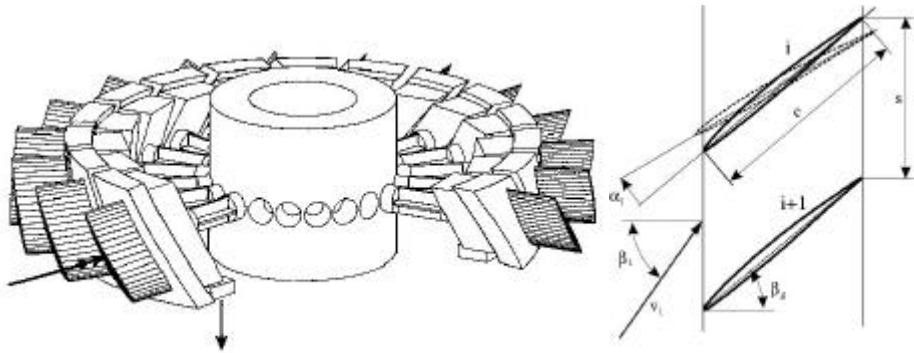


Figure 1: Cross-section of the annular cascade tunnel ([2])

The advantage of the wind tunnel is the possibility to investigate the aeroelastic behaviour of a cascade in a non-rotating test facility. Fig. 1, taken from [2] shows the cross-section of the wind tunnel. A spiral flow is generated in order to simulate real inflow angles such as those which occur in rotating cascades. The flow angle in the test section can be regulated from 30° to 78° and the inlet Mach number can be varied between 0.3 and 1.4 [2].

Steady conditions are measured by aerodynamic probes in the upstream and downstream sections and by pressure taps on the blade surfaces. The aerodynamic probes were calibrated to measure the total pressure p_{t1} p_{t2} , the steady pressures p_1 and p_2 , and the flow angles β_1 and β_2 . The values were measured at the radial positions $0.13 \leq z/h \leq 0.83$ in steps of $\Delta z/h = 0.1$ by moving the probe and at the circumferential positions $0^\circ \leq \varphi \leq 27^\circ$ in steps of 1° by rotating the cascade.

The test vehicle is a transonic annular cascade consisting of 20 NACA3506 airfoils with chord length of 80mm, a stagger angle of 40° and a pitch at midspan of 65mm. The blades are mounted via elastic spring suspensions which allow a torsional motion around midchord. The airfoils were excited in travelling wave modes, performing tuned torsional vibrations at 220 Hz with a constant interblade phase angle between adjacent blades. The blade vibration amplitudes reached approximately 0.3° (see *fig. 2*). Experiments were run for sub- and transonic flow conditions, with steady traverses taken at the in- and outlet planes. Furthermore, steady pressure taps were used on three radial stations of different blades to acquire surface static pressure distributions.



(a) Cut-away view of the annular cascade (b) Cascade geometry

Figure 2

26 unsteady pressure transducers were mounted at mid-span blade sections, with 16 transducers on the suction and 10 on the pressure side. To give a good resolution of the unsteady pressure distribution around the shock for the transonic case, eight transducers were clustered in the front half of the suction side. A detailed discussion of the measurements is given by Hennings and Belz [1,7].

4 Computational methods

3.1 STEADY EULER METHOD

For steady inviscid calculations, a 3D Euler code developed at MTU is used [6]. It uses a Finite-Volume scheme with a 3-step Runge-Kutta time integration method. A special feature is its ability to model secondary in- or outflow, such as bleed- or cooling flows in a multi-stage turbomachine. This code was also used as a basis for the design of the time linearized unsteady Euler method described below. Furthermore, the results of the steady Euler code are used as the base flow for the time linearized Euler code.

3.2 STEADY NAVIER-STOKES METHOD

To assess the influence of viscous effects and of the tip leakage flow, the steady Navier-Stokes method TRACE_S was used. This method was developed in co-operation between DLR Cologne and MTU.

The block-structured code uses a cell-centred explicit finite-volume to solve the Reynolds-averaged Navier-Stokes equations formulated in relative Cartesian co-ordinates. The code employs a time-marching Runge-Kutta scheme along with matrix dissipation to minimise corruption of solutions by numerical smoothing. To speed up convergence to steady state, successive mesh refinement, residual smoothing, and local time-stepping are applied. Turbulence models, beyond the algebraic Baldwin-Lomax model, include the standard k - ϵ model, the Cato-Launder variant thereof, a low Reynolds k - ϵ model, and a k - ω model. Details of the method can be found in [5].

3.3 UNSTEADY TIME LINEARIZED EULER METHOD

The unsteady calculations were performed using the 3D time linearized Euler Method Lin3d. It is based on the linearisation of the steady Euler method described above and is an extension of the method described in [8,9]. Lin3d is a fast and robust tool routinely used in the design process to assess flutter stability and forced response of compressor and turbine bladings. It features deforming meshes, non-reflecting boundary conditions, arbitrary eigenmodes (including chordwise bending), forced-response calculations for generalised forces due to up- and downstream disturbances and the possibility of calculation of acoustic modes. Lin3d runs on a wide variety of platforms ranging from workstations to multiprocessor vector supercomputers, with the option of parallel computing to speed up the turnaround times.

5 Discussion of Results

A prerequisite for a successful unsteady calculation is the proper modelling of the steady flow field. This is especially important for the unsteady linearized methods as the one used here, where the steady flow is used as the base flow around which the linearisation is performed, but the statement also holds true for non-linear calculations. When trying to model an experiment such as the one used here, a calculated steady flow that is significantly off the measured values will very likely also lead to unsteady calculation results that are useless. For the current case, previous investigations using a fairly sophisticated quasi-3D non-linear Navier-Stokes method [4] have highlighted severe problems in achieving the goal of modelling the measured steady pressure distribution around the blades.

5.1 STEADY FLOW WITHOUT SECONDARY INFLOW

The first attempt to model the steady experimental flow field was performed using the steady 3D Euler method described above. At the inflow boundary, total temperature, total pressure and the radial and circumferential flow angles have to be prescribed for this method. Of these values, the total pressure and circumferential flow angles are known from the experimental scans from a relative blade height of 13% up to 83%. The total temperature was assumed to be constant, the radial flow angle was assumed to be zero. For the near-hub and near-tip regions, a reasonable boundary layer profile was assumed for the calculations. At the outlet, the static pressure at midspan was prescribed as taken from the experiments, the radial distribution from hub to tip was deduced from the resulting flowfield with the assumption of simple radial equilibrium.

The results of this first attempt are shown in *fig. 3*. The symbols denote the measured values at midspan, the dashed lines are the results of the steady 3D Euler calculation with the above mentioned parameters. Since the radial variation of the results is rather small, only the midspan data is shown here.

It is obvious that the measured values indicate a lightly loaded, completely subsonic cascade, while the computation yields much higher loading with a strong shock in the passage. The results from Navier-Stokes calculations with similar boundary conditions were only marginally different from these Euler results. Changing the inflow profile in the region from 0% to 13% span and from 84% to 100% span,

where no measured values are available, also showed only a minor influence on the resulting flow field. Since the used methods are well calibrated and are known to be fairly accurate, it was felt that some other important effect must be present that had so far eluded us.

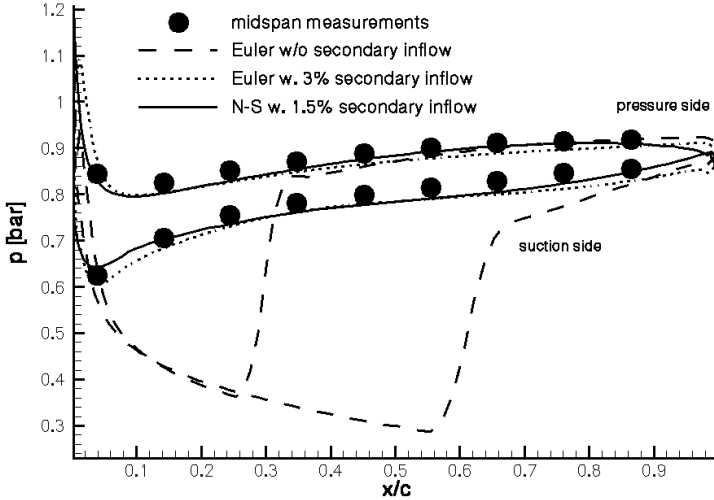


Figure 3: Comparison of measured and calculated steady midspan pressure distributions.

One candidate for such an effect is the tip leakage flow. Since the blades are spring-mounted at the hub and free to oscillate, a small tip gap is inevitable. In the experiment, the size of the gap was approximately 0.25 mm. However, when including the tip gap in the Navier-Stokes calculations, only a fairly small effect, localised at the region from approximately 90% to 100% span was visible. The overall loading of the cascade and consequently the overall turning, was still way too high. Increasing the tip gap in the computation up to a value of 1 mm did not fundamentally change this picture.

5.2 ESTIMATE OF THE SECONDARY INFLOW MAGNITUDE

The design of the oscillating cascade necessitates small gaps between the platforms of adjacent blades in the cascades to allow the individual blades to oscillate freely at arbitrary interblade phase angles, pictured in fig. 4. The inner area of the set-up forms a barrel (see fig. 2a) that is vented to atmospheric conditions by a number of holes in the cover-plates at the top and bottom of this barrel. The static pressure on the hub contour of in the blade channel on the other hand would be lower than

atmospheric due to the fairly high Mach numbers. Hence it was felt that the pressure difference across the gaps between the blade platforms could lead to a leakage flow into the cascade that might have an effect on the overall flow field.

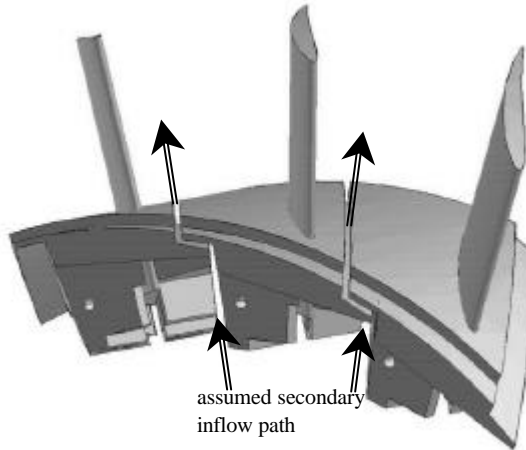


Figure 4: Detail view (in direction of the main flow) of the gap between the oscillating blade platforms.

To estimate the magnitude of this secondary inflow, the pressure difference over the gaps and the gap geometry are needed. The geometry is known from the design, the pressure difference was taken from static pressure measurements inside the barrel and from an extrapolation of the blade surface measurements to the hub contour. Using a simple through-flow correlation for the current gaps of 0.5mm minimum width and 80mm length yields a massflow of only 8g/s for each slot. This seems to be very small, but for 20 slots and an overall massflow through the cascade of approximately 8 kg/s it adds up to 2% of the total massflow. Taking into account the rather crude assumptions used for this estimate, it is felt that a range of 1% to 3% secondary inflow is a realistic value for this experiment.

5.3 STEADY FLOW WITH SECONDARY INFLOW

To assess the effect of the presumed secondary inflow, additional steady calculations were performed. In *fig. 3*, the dramatic effect that this seemingly minor change has on the overall flowfield becomes obvious. The dotted lines show the results of the Euler calculation with 3% secondary inflow. It is seen that the static pressure distribution now matches the measured values over the whole blade surface fairly well.

This is also reflected in the overall flow turning, which now matches the measured value to within 1° . Similarly, the Navier-Stokes calculations with only 1.5% secondary inflow (shown as solid lines in *fig. 3*) yield an even better agreement with the measured values.

Closer examination of the flowfield with secondary inflow reveals the main effect that leads to this significant change in the overall behaviour of the cascade. *Fig. 5* shows the Mach-number contours of the Navier-Stokes calculation with 1.5% secondary inflow. Displayed are planar cuts on planes of $x=const.$ through two passages near the leading edge (*a*), at midchord (*b*) and near the trailing edge (*c*). It is seen that the low-velocity fluid coming in through the slot in the hub contour penetrates a large region from the hub of the cascade up to almost midspan.

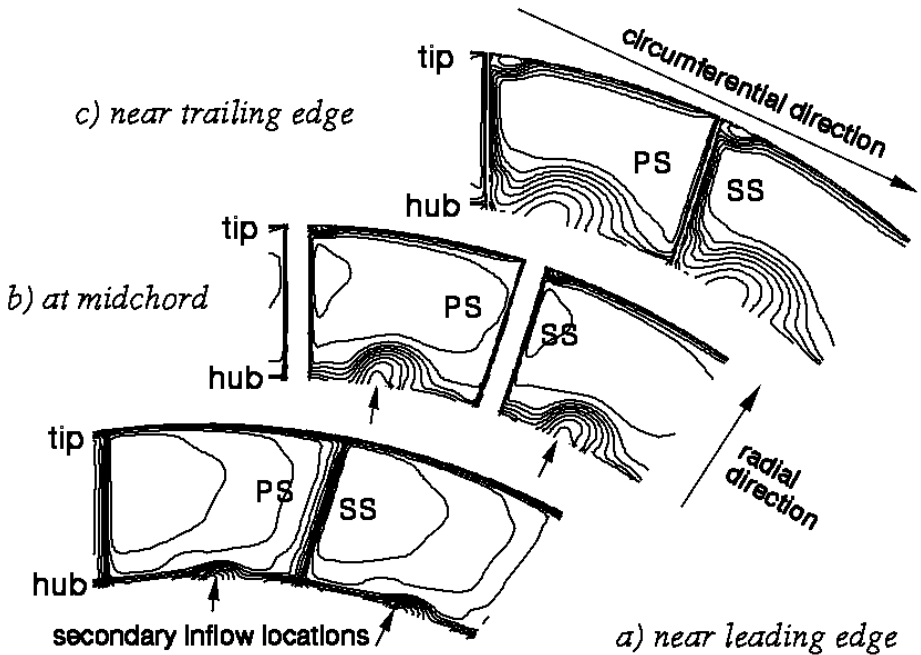


Figure 5: Mach number distributions on $x=const$ planes showing the influence of secondary inflow

This leads to a redistribution of the main flow towards the tip of the cascade, where a significant streamtube contraction takes place. The contraction increases the axial velocity of the main flow, reduces the turning and hence leads to a strong unloading of the cascade. The different behaviour of Euler- and Navier-Stokes-calculations is also consistent with this picture. In the Navier-Stokes-calculations, the hub-

and casing boundary layers tend to increase the streamtube contraction in the midspan region, hence a smaller amount of secondary inflow (1.5%) leads to results that are very similar to the Euler-calculations with a higher secondary inflow (3%).

5.4 UNSTEADY FLOW

It was previously stated that a good representation of the steady (or time-mean) flowfield is imperative to a successful modelling of the unsteady flow. From the discussion of the influence of secondary inflow on the steady flowfield, it may seem obvious that an unsteady calculation based on the solution without secondary inflow would lead to erroneous results. However, in many situations in a real turbomachine, the “true” surface pressure distributions on the blades will not be known, since they are not measured, so that the results from a steady calculation with measured boundary conditions have to be taken for granted. Assuming such a situation, unsteady calculations were performed based on the steady Euler flow without secondary inflow.

Figure 6a displays the magnitudes of the pressure coefficients resulting from this computation. The magnitudes are shown as a carpet plot for all 20 interblade phase angles σ over the relative chord length x/c along the suction side (left) and the pressure side (right). Comparing these plots with the experimental results, shown in *fig. 6b*, it is obvious that there is little correlation between these two. While the computed distributions are dominated by the shock impulses at $x/c \approx 0.6$ on the suction side and $x/c \approx 0.25$ on the pressure side, the experimental values show a smooth distribution with peak values in the leading edge region.

In the present situation, the knowledge of the measured steady surface pressures enables us to use the well matched Euler solution with 3% secondary inflow as shown in the above section. This leads to the unsteady results shown in *fig. 6c*. The overall shape as well as the leading edge maxima of the pressure coefficient magnitude distribution are now closely reproduced by these computational results, and this also holds true for the phases shown in *fig. 7*. Here, only the measured and the Euler results with secondary inflow are shown.

While the overall agreement is rather satisfying, some details are worth a closer inspection. First, the experiments show a strong change in the magnitudes as well as in the phases between the interblade phase angles of 18° and 36° . This is also seen in the computational results, although the magnitudes at 36° are overpredicted by the computation.

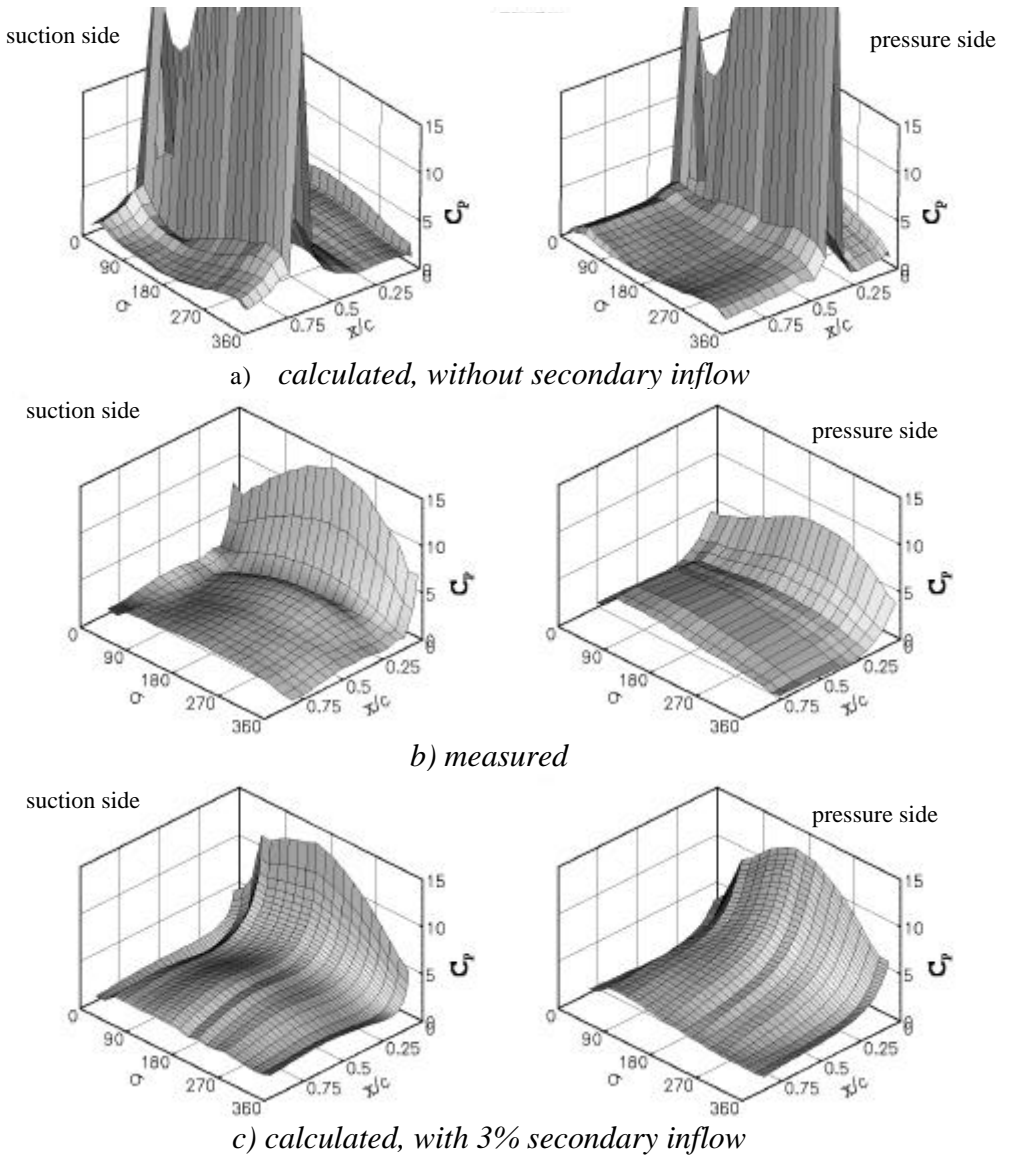


Figure 6: Unsteady pressure coefficient magnitudes

This behaviour can be traced to an acoustic resonance condition in the inlet region at $\sigma \approx 30^\circ$. Since the linearized Euler method is equipped with fully non-reflecting boundary conditions, this cut-on/cut-off change is very pronounced. In the experiment, the inflow section of the wind tunnel will most certainly produce some reflections of the acoustic wave, which tends to smear out the discontinuity, just as seen in the experimental results.

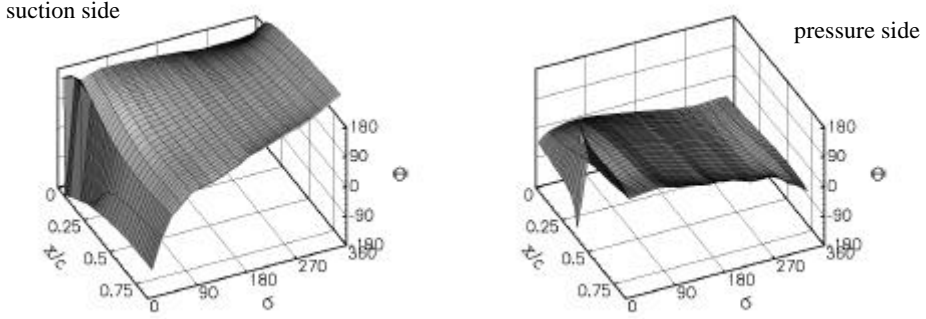
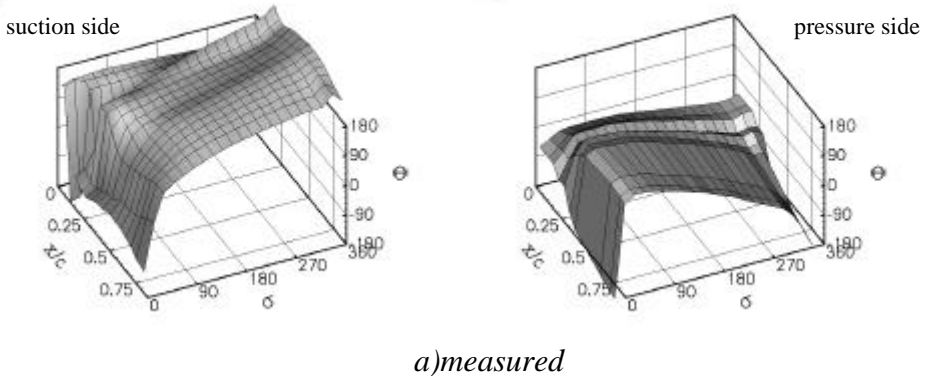


Figure 7: Unsteady pressure coefficient phases F

Another point worth noting is seen in the unsteady pressure distributions for interblade phase angles near 180° , shown in detail in *fig. 8*. In this figure, the symbols denote the measured values while the lines are the results of the computation. The magnitudes are shown as solid lines and squares, the phases as dashed lines and triangles, respectively. Finally, suction the side is shown on the left and the pressure side on the right.

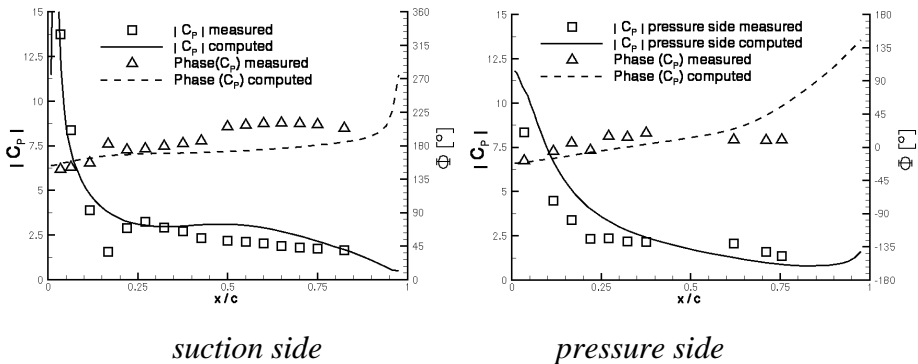


Figure 8: Unsteady pressure coefficient distributions for $s=180^\circ$.

Although the overall agreement between measurement and computation is seen to be quite good, the measured suction side magnitudes show a sharp decrease at approximately 15% chord length, while the calculated values do not show this drop at all. This behaviour is seen in a wide range of interblade phase angles around 180° . Similarly, the measured phase at this location seems to fall out of line with the neighbouring transducers. Taking a closer look at *fig. 7a (left)*, the same is found for almost all values the interblade phase angle \mathcal{S} . Mesh refinement of the computational grid and other changes in the computational parameters have been tried to improve the agreement in this region, but the effects were very minor. At the present time, it is not clear if some physical phenomenon that is not modelled correctly is at work here or if the pressure measurements were flawed for this transducer

6 Conclusions

Steady and unsteady computations have been performed for an annular oscillating compressor cascade, for which high-quality steady and unsteady experimental data is at hand.

Based on previously experienced problems in modelling the measured steady flow conditions, the influence of three-dimensionality, viscosity, tip leakage, boundary conditions and secondary inflow was studied. It was found that only the assumption of a secondary inflow through the gaps between the cascade hub platforms in the region of 1.5% - 3% of the total mass flow leads to a good agreement between measured and computed steady pressure distributions. This value was shown to be consistent with a through-flow estimate based on the gap geometry and the measured static pressure difference across the gap. Using a sophisticated Navier-Stokes method with the inclusion of tip leakage flow was shown to further improve the calculated pressure distributions, but these were found to be minor changes.

When performing unsteady calculations, it was found to be of utmost importance to use the correct steady base flow, as the computation did otherwise yield nonsensical results. Based on the correct steady flow, the unsteady results yielded good overall agreement with the measured local unsteady surface pressures in terms of magnitude and phase angle. The overall results support the conclusion that the linearised solver is able to model the dominant unsteady effects for this case, if the underlying base flow resembles the real flow field well enough.

7 References

- 1 Belz, J. and Hennings, H.: Aerodynamic Stability Investigations of an Annular Compressor Cascade Based on Unsteady Pressure Measurements, *ISUAAAT conference, Lyon, 5.-9.Sept. 2000, to be published by Kluwer Academic Publishers.*
- 2 Bölcs, A.: A Test Facility for the Investigation of Steady and Unsteady Transonic Flows in Annular Cascades, *ASME-83-GT-34*, 1983.
- 3 Bölcs, A. and Fransson, T.H.: *Aeroelasticity in Turbomachines: Comparison of Theoretical and Experimental Cascade Results.* Communication du Laboratoire de Thermique Appliquée et de Turbomachines Nr. 13, L'Ecole Polytechnique Fédérale de Lausanne, 1986.
- 4 Carstens, V. and Schmitt, S.: Comparison of Theoretical and Experimental Data for an Oscillating Transonic Compressor Cascade, *ASME-paper 99-GT-408*, 1999.
- 5 Fritsch, G., Hoeger, M., Blaha, C. and Bauer, D.: Viscous 3D Compressor Simulations in Parallel Architectures – Design Tool Development and Application to a Transonic Compressor Stage. *AIAA-paper 97-2876*, 1997.
- 6 Happel, H.-W. and Stubert, B.: Computation of Transonic 3D Cascade Flow and Comparison with Experiments, *AGARD-CP-437*, 1988.
- 7 Hennings, H. and Belz, J.: Experimental Investigation of the Aerodynamic Stability of an Annular Compressor Cascade Performing Tuned Pitching Oscillations in Transonic Flow, *ASME-paper 99-GT-407*, 1999.
- 8 Kahl, G. and Klose, A.: Computation of Time Linearized Transonic Flow in Oscillating Cascades, *ASME-93-GT-269*, 1993.
- 9 Kahl, G.: Application of the Time Linearized Euler Method to Flutter and Forced Response Problems, *ASME-95-GT-123*, 1995.
- 10 Körbächer, H. and Bölcs, A.: Steady-State and Time-Dependent Experimental Results of a NACA-3506 Cascade in an Annular Channel, *ASME-96-GT-334*, 1996.
- 11 Nowinski, M. and Panowsky, J.: Flutter Mechanisms in Low Pressure Turbine Blades, *ASME-98-GT-573*, 1998.